The Korean Journal of Ceramics, 1 [4] 204-208 (1995)

Electrical Properties of $Ba_{1-x}Sr_xTiO_3$ Thin Films Deposited by Metalorganic Chemical Vapor Deposition

Jong-Guk Yoon, Soon-Gil Yoon, Won-Jea Lee* and Ho-Gi Kim*

Dept. of Mater. Eng., College of Eng., Chungnam Nat. Univ., Deaduk Sci. Town, Teajon 305-764, Korea.
**Dept. of Ceram. Sci. & Eng., Korea Advanced Institute of Sci. and Tech., Teajon 305-701, Korea.*
(Received October 24, 1995)

The microstructure and electrical properties were investigated for polycrystalline $Ba_{1-x}Sr_xTiO_3$ (BST) thin films deposited on Pt/Ti/SiO_2/Si(PTSS) and Pt/MgO(PM) substrates by metalorganic chemical vapor deposition (MOCVD). BST films on PTSS have columnar and porous structures, while on PM have an equiaxied and dense structure. The dielectric constant and a dissipation factor of BST films on PTSS and PM were 365, 0.05 and 205, 0.02 at 100 kHz, respectively. A charge storage density of 20 fC/μm^2 on PTSS and 12 fC/μm^2 on PM was obtained at an applied electric field of 0.06 MV/cm. Leakage current density of BST films on PM was smaller than that on PTSS. The leakage current density level was about 8×10^{-8} A/cm^2 at 0.04 MV/cm.

Key words : MOCVD, BST, Electrical properties, Microstructure

I. Introduction

Ferroelectric thin films such as $Pb(Zr,Ti)O_3$,[1] $SrTiO_3$,[2] and $(Ba,Sr)TiO_3$(BST)[3,4] are highly attractive as a key material for 256 Mb and 1 Gb dynamic random access memories (DRAMs). Among these materials, BST is the most promising capacitor material for DRAM use because the films have high dielectric constant with lower leakage current level.

Various deposition techniques such as radio-frequency magnetron sputtering,[5] laser ablation,[6] and metalorganic chemical vapor deposition(MOCVD)[7] have allowed successful synthesis of BST films. Among these techniques, the MOCVD method is a promising process because of its potential advantages such as the ability to deposit high-quality and the amenability to large-scale processing. In this study, BST thin films were fabricated by MOCVD with different substrates and the effect of substrates on electrical properties were evaluated.

II. Experimental Procedure

The success of any MOCVD process depends critically on the volatility and stability of the precursor material. $Ba(hfa)_2$(tet) and $Sr(hfa)_2$(tet) exhibit significantly improved volatility and vapor pressure stability in comparison to other precursors.[8] The metalorganic precursors used in this work were $Ba(hfa)_2$(tet) and $Sr(hfa)_2$(tet) [(hfa =hexafloroacetyl-acetonate; $C_5HF_6O_2$); (tet=tetraglyme)] for the barium and strontium source, respectively. Titanium tetraisopropoxide (TPT) was also chosen as the Ti source. The deposition conditions of BST films were shown in Table 1. BST films were deposited on Pt(150 nm)/Ti(50 nm)/SiO_2/Si(PTSS) and Pt(100 nm)/MgO(PM) substrates. The film thickness was determined by using the cross-section scanning electron microscopy (SEM). X-ray diffraction (XRD) using Cu Kα radiation was used to determine the crystal phase and preferred orientation of the films. The dielectric and electrical properties of the BST films were evaluated by capacitance-frequency (C-F), current-voltage (I-V), and capacitance-voltage (C-V) plots. They were carried out in a metal-insulator-metallic (MIM) configurations, where the top electrode of Pt with a diameter of 0.3 mm were prepared by dc sputtering.

III. Results and Discussion

1. Film structure

Fig. 1 shows the XRD patterns of BST films deposited on PTSS and PM at 850°C. From Fig. 1, BST films deposited on PTSS and PM have polycrystalline single phase. Figs. 2 and 3 show the relationship between the texture coefficient and the deposition temperatures of as grown BST films deposited on PTSS and PM. In order to investigate the preferred orientation of the deposition layer, texture coefficient TC (hkl) of each plane is obtained using the Harris method[9] as follows;

$$TC(hkl)=\frac{I(hkl)}{I_0(hkl)}\left[\frac{1}{n}\sum_{1}^{n}\frac{I(hkl)}{I_0(hkl)}\right]^{-1} \quad (1)$$

Where I_0(hkl) is the standard intensity of the (hkl) plane, I_0(hkl) is the measured intensity of the (hkl) plane, and n is the number of reflections. Equation (1) shows that TC(hkl) of each crystal plane is unity for a randomly distributed powder sample while TC (hkl) of each

Table 1. Deposition Conditions for BST Preparation

Bubbling Temperature of $Ba(hfa)_2$ tet*	120°C
Ar Carrier Gas Flow Rate of Ba	80 sccm
Bubbling Temperature of $Ba(hfa)_2$ tet.	120°C
Ar Carrier Gas Flow Rate of Sr	80 sccm
Bubbling Temperature of $Ti(O\text{-}iC_3H_7)_4$	30°C
Ar Carrier Gas Flow Rate of Ti	20 sccm
O_2 Gas Flow Rate	200 sccm
Total Flow Rate	400 sccm
Growth Temperature	800-900°C
Growing Time	3 h
Growth Pressure	4 Torr
Substrate	Pt/MgO
	$Pt/Ti/SiO_2/Si$

*hfa: hexafluoroacetylacetonate.
tet.: tetraglyme.

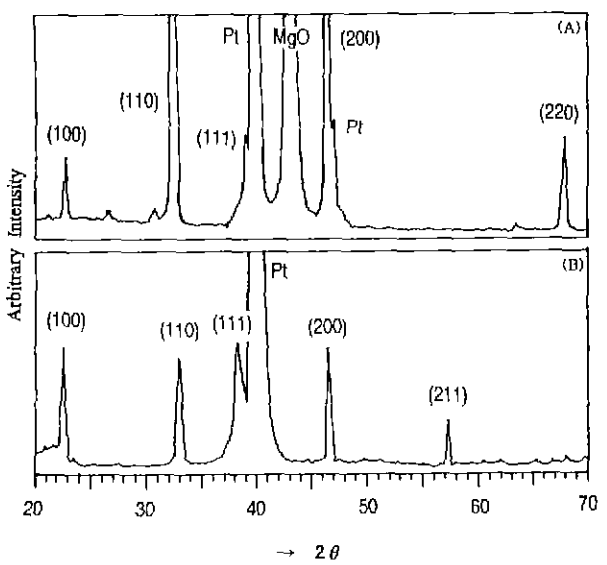

Fig. 1. XRD patterns of BST films deposited on (A) PM and (B) PTSS at 850°C.

crystal plane is larger than unity for the preferred growth.

Texture coefficient analysis on PTSS reveals that the BST deposit has (100) preferred orientation as deposition temperatures increase. However, BST films on PM have (111) preferred orientation below 850°C and (100) orientation above 850°C. The growth direction of BST films on PM switches from (111) to (100) as deposition temperature increases. We could suggest that BST film grows with (100) preferred orientation regardless of substrate types as the deposition temperature increases. Fig. 4(A) and (B) show the cross-sectional SEM images of BST films deposited on PTSS and PM substrates respectively. BST on PM has the equiaxied and dense structure, while on PTSS shows the c-axis grown columnar and a little porous structure. The microstructure of BST films on two different substrates affects the electrical properties.

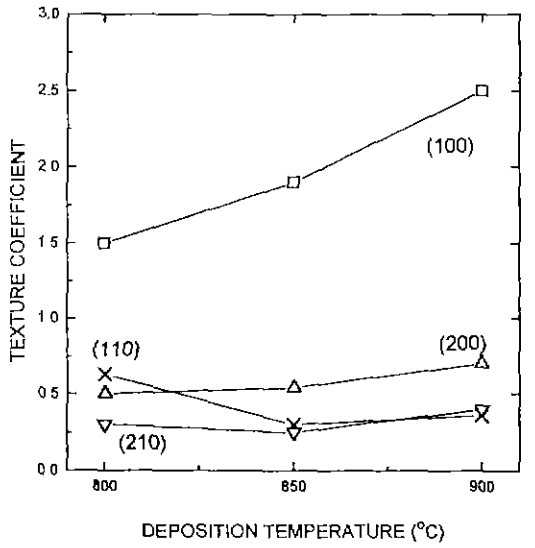

Fig. 2. Texture coefficient of BST films deposited on Pt/Ti/SiO_2/Si with various deposition temperatures.

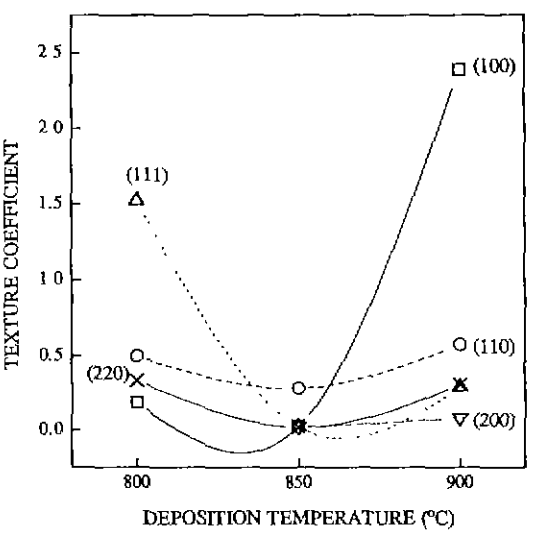

Fig. 3. Texture coefficient of BST films on Pt/MgO with various deposition temperatures.

2. *Electrical properties*

Fig. 5 shows the variation of dielectric constant and dissipation factor (tanδ) as a function of frequency. The dielectric constants of BST on PM and PTSS were almost constant regardless of applied frequency. However the dielectric constant and the dissipation factor of BST on PTSS were larger than those of PM. Larger dissipation factor of BST on PTSS than that of BST on PM

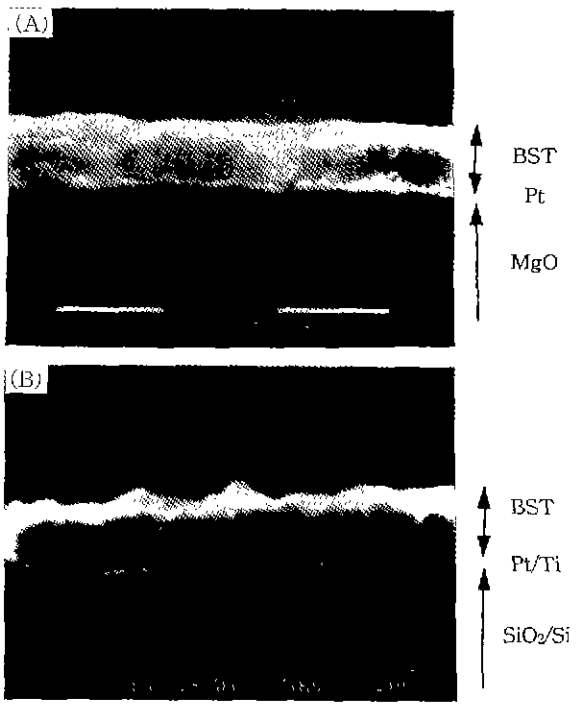

Fig. 4. Cross-sectional image of BST films deposited on (A) Pt/MgO and (B) Pt/Ti/SiO_2/Si at 900°C.

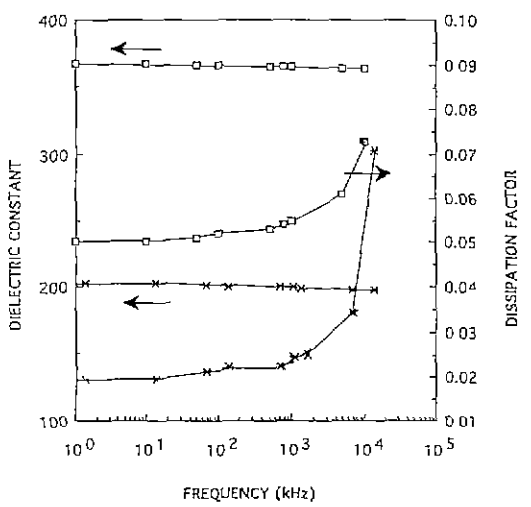

Fig. 5. Dielectric constant and dissipation factor of BST film deposited at 900°C as a function of frequency. (—⊡—⊡—: BST/Pt/Ti/SiO_2/Si, —✳—✳—: BST/Pt/MgO).

could explain as follows. BST films on PTSS have a columnar and a porous structure as shown in SEM morphology. They have many defects (vacancy, mobile ions). The charges trapped at these defects increased the dissipation factor because they can not keep up with the increase of the frequency. BST films deposited on PTSS and PM have a dielectric constant of 365 and 205, dissipation factor of 0.05 and 0.02 at 100 kHz frequency, respectively.

Fig. 6 shows the capacitance vs voltage characteristics

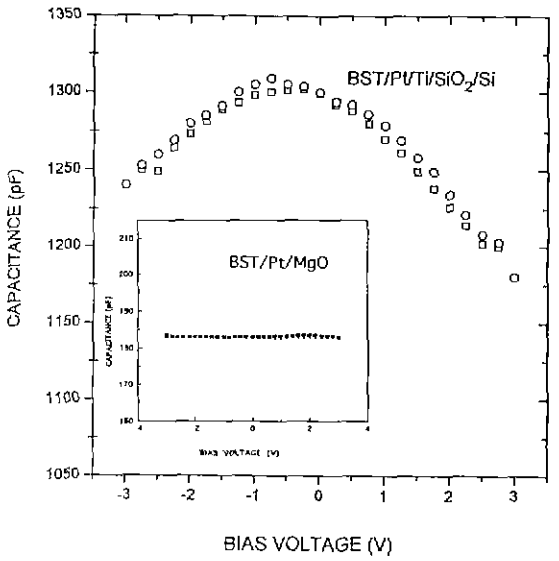

Fig. 6. Capacitance-voltage characteristics of BST film deposited at 900°C(electrode diameter: 0.3 mm, film thickness: 500 nm, frequency: 100 kHz).

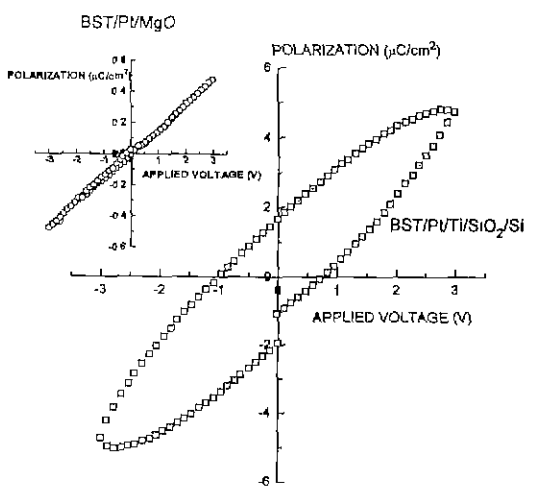

Fig. 7. P-E curves of BST films deposited on PM and PTSS.

of BST films deposited on PTSS at 900°C. Capacitance-Voltage measurements were performed at 100 kHz. It is seen that the capacitance was largely affected by the electric field within the region of applied voltage ±3V. The voltage of maximum capacitance shifted between -0.75 to -0.25 V both for increasing and decreasing bias voltage. Capacitance-Voltage characteristics shows asymmetric behavior with bias voltage. This result was due to movement of space charges in thin films. The fact that BST films deposited on PTSS have a linear dielectric properties was shown in P-E curve of Fig. 7. Asymmetric behavior of BST/PTSS was due to the difference of interfacial properties of Pt/BST and BST/Pt experienced different thermal hystories. The BST deposition was performed at the same condition for PM and PTSS. The reason for difference of P-E curve will be studied in detail

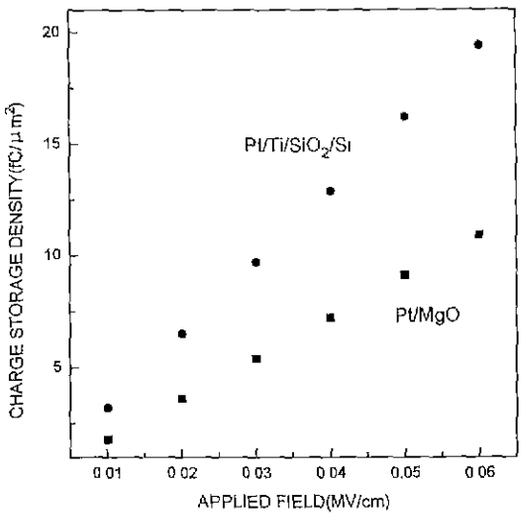

Fig. 8. Charge storage density of BST film as a function of applied field.

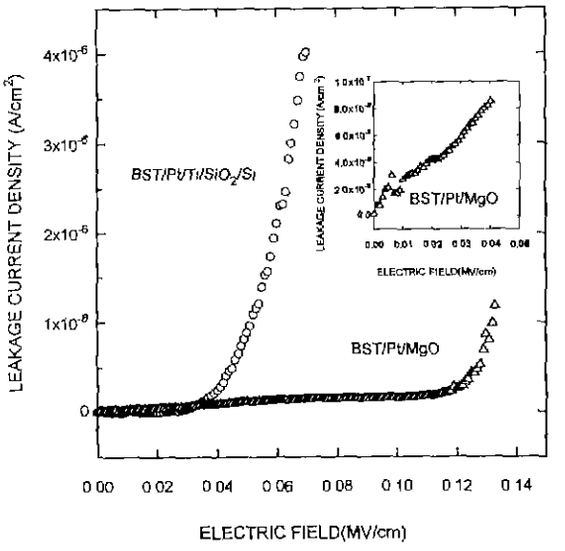

Fig. 9. Leakage current density of BST film deposited at 900°C as a function of applied field.

through the compositional analysis of BST films. The inset of Fig. 6 shows the C-V characteristics of BST films deposited on PM. From this result, we could explain that the BST films on PM have paraelectric properties at room temperature. Because BST films have paraelectric properties at room temperature, we can calculate the charge storage density Qc using the following equation :

$$Q_c = \varepsilon_0 \cdot \varepsilon_r \cdot E$$

Where ε_0 and ε_r are the dielectric permittivity of vacuum and the dielectric constant of $(Ba,Sr)TiO_3$ films, respectively. E is the applied electric field. The relation between applied electric field and the calculated charge storage density is shown in Fig. 8. The charge storage density was calculated from capacitance-voltage measurements of BST films. BST films deposited on PM and PTSS have a Qc of about 12 fC/μm² and 20 fC/μm² at 0.06 MV/cm, respectively.

Fig. 9 shows the I-V characteristics of the BST film deposited on different substrates. As shown in Fig. 9, leakage current density of BST on PTSS abruptly increases at lower electric field than that of BST on PM. Leakage current behavior of BST on PTSS may be explained in terms of charge carrier traps. As shown Fig. 4(B), this film has porous and columnar microstructure which might have a number of carrier traps. In the low electric field region, carriers are localized around the traps reducing leakage current density(J). At the high electric field region, the localized carriers begin to come out of the trap, resulting in an abrupt increase of J. However, leakage current density of BST on PM was smaller than that on PTSS. As shown in Fig. 4(A), BST films have equiaxied and random orientation. This structure plays a decisive role as the barrier of leakage current path. As shown in inset of Fig. 9, at low voltages, the leakage current density is virtually linear. However, at high voltages, the leakage current becomes nonlinear. The I-V characteristics at low-fields indicated that the ohmic behavior of current flow is dominant in this regions. The nonlinear relationship in the high voltage region suggested other conduction mechanisms. Conduction mechanisms will be studied through detailed experiments afterward.

IV. Conclusions

The polycrystalline $Ba_{1-x}Sr_xTiO_3$ thin films were successfully grown on PTSS and PM substrates by MOCVD technique. The microstructure of BST films deposited on two different substrates affects the electrical properties. BST films deposited on PTSS exhibited columnar structure, dielectric constant of 365, dissipation factor of 0.05 at 100 kHz, and charge storage density of 20 fC/μm² at 0.06 MV/cm. The leakage current characteristics of BST films on PM are superior to those of films on PTSS. Leakage current density of films deposited on PTSS and PM is about 5×10^{-7} A/cm² and 8×10^{-8} A/cm² at 0.04 MV/cm, respectively.

References

1. M. Shimizu, M. Fujimoto, T. Katayama, T. Shiosaki, K. Nakaya, M. Fukagawa, and E Tanikawa, "Growth and Characterization of Ferroelectric $Pb(Zr,Ti)O_3$ Thin Films by MOCVD Using a 6 inch Single Wafer CVD System," *Mater. Res. Soc. Symp. Proc.* 310, 255 (1993).
2. S. Liang, C. S. Chern, and Z. Q. Shi, "Epitaxial Growth of $SrTiO_3/YBa_2Cu_3O_{7-x}$ Heterostructures by Plasma-enhanced Metalorganic Chemical Vapor Deposition," *Appl. Phys. Lett.* **64**[26], 27 June, 3563 (1994).
3. T. Horikawa, N. Mikami, T. Makita, J. Tanimura, M. Kataoka, K. Sato, and M Nunoshita, "Dielectric Properties

of (Ba,Sr)TiO_3 Thin Films Deposited by RF Sputtering," *Jpn. J. Appl. Phys.* **32**, 4126 (1993).

4. C. S. Chern, S. Yoon, and A. Safari, "Heteroepitaxial Growth of $Ba_{1-x}Sr_xTiO_3/YBa_2Cu_3O_{7-x}$ by Plasma-Enhanced Metalorganic Chemical Vapor Deposition," *Appl. Phys. Lett.* **64**[23], 6 June, 3181 (1994).
5. N. Ichinose and T. Ogiwara, "Preparation and Properties of (Ba,Sr)TiO_3 Thin Films by RF Magnetron Sputtering," *Jpn. J. Appl. Phys.* **32**, 4115 (1993).
6. S. G. Yoon, J. C. Lee, and A. Safari, "Preparation of Thin Films $(Ba_{0.6},Sr_{0.5})TiO_3$ by the Laser Ablation Technique and Electrical Properties," *J. Appl. Phys.* **76**[5], 1 September, 2999 (1994).
7. T. Kawahara, M. Yamamuka, T. Makita, J. Naka, A. Yuuki, N. Mikami, and K. Ono, "Step Coverage and Electrical Properties of (Ba,Sr)TiO_3 Films Prepared by LSCVD using $TiO(dpm)_2$," *Jpn. J. of Appl. Phys.*, **33**[9B], 5129 (1994).
8. L. A. Wills, B. W. Wessels, D. S. Richeson, and T. J. Marks, "Epitaxial Growth of $BaTiO_3$ Thin Films by Organometalic Chemical Vapor Deposition," *Appl. Phys. Lett* **60**[1], 6 January, 41 (1992).
9. C. Barret, and T. B. Massalski, "Structure of Metals" P 204, Pergamon Press, Ltd, Oxford (1980).